Biomaterials 33 (2012) 5638–5649

Contents lists available at SciVerse ScienceDirect

Biomaterials

journal homepage: www.elsevier.com/locate/biomaterials

The prolonged survival of fibroblasts with forced lipid catabolism in visceral fat following encapsulation in alginate-poly-L-lysine

Fangping Yang [a], Xulang Zhang [b], Andrei Maiseyeu [c], Georgeta Mihai [d], Rumana Yasmeen [e], David DiSilvestro [a], Santosh K. Maurya [d], Muthu Periasamy [d], K. Valerie Bergdall [e], Gregg Duester [f], Chandan K. Sen [c], Sashwati Roy [c], L. James Lee [b,1], Sanjay Rajagopalan [c,1], Ouliana Ziouzenkova [a,*]

[a] Department of Human Nutrition, The Ohio State University, Columbus, OH, USA
[b] NSF Nanoscale Science and Engineering Center for Affordable Nanoengineering of Polymeric Biomedical Devices, The Ohio State University, Columbus, OH, USA
[c] Davis Heart and Lung Research Institute, The Ohio State University, Columbus, OH, USA
[d] Department of Physiology & Cell Biology, The Ohio State University, Columbus, OH, USA
[e] University Laboratory Animal Resources, The Ohio State University, Columbus, OH, USA
[f] Development and Aging Program, Sanford-Burnham Medical Research Institute, La Jolla, CA, United States, 92037, USA

ARTICLE INFO

Article history:
Received 24 February 2012
Accepted 12 April 2012
Available online 9 May 2012

Keywords:
Vitamin A
Aldehyde dehydrogenase
Abdominal obesity
Insulin resistance
Magnetic resonance imaging
Laser capture microdissection
Alginate-poly-L-lysine
Uncoupling protein 1
Thermogenesis
Lipolysis
Retinoids

ABSTRACT

Although alginate-poly-L-lysine (AP_L) encapsulation of cells producing bioactive peptides has been widely tested, it is unknown whether AP_L supports lasting catabolic functions of encapsulated cells in adipose tissue, which are required for obesity reduction. We tested functions of AP_L-encapsulated fibroblasts isolated from wild-type (WT) and aldehyde dehydrogenase 1a1 knockout mice (KO), which resist obesity on a high-fat (HF) diet, have a higher metabolic rate, and express increased levels of thermogenic uncoupling protein-1 (Ucp1) in their deleterious visceral fat depots compared to WT mice. To enable in vivo detection and quantification, fibroblasts were stably transfected with green-fluorescent protein. WT- or KO-containing microcapsules were injected into two visceral depots of WT mice fed an HF diet. Eighty days after transplantation, microcapsules were located in vivo using magnetic resonance imaging. KO microcapsules prevented weight gain in obese WT mice compared to a mock- and WT capsule-injected groups on an HF diet. The weight loss in KO-treated mice corresponded to lipid reduction and induction of thermogenesis in the injected visceral fat. The non-treated subcutaneous fat was not altered. Our data suggest that the AP_L polymer supports long-term catabolic functions of genetically-modified fibroblasts, which can be potentially used for depot-specific obesity treatment.

1. Introduction

Microcapsules fabricated from alginate-poly-L-lysine (AP_L) were established as delivery vehicles for engineered cells producing bioactive peptides, such as insulin, leptin, and growth factors [1–4]. In contrast, the ability for AP_L microcapsules to support the long-term survival and functions of cells catabolizing metabolites has not been examined. Application of encapsulated catabolically-active cells will require different strategies for microcapsule tracking, monitoring transplanted cell viability, functions, and interaction with the host cells. Metabolic disorders, especially obesity, can benefit from the engraftment of cells with forced lipid utilization, energy dissipation, and/or high metabolic rate.

Obesity in humans and rodents is a multifactorial disorder depending on genetic factors, diet, energy expenditure, and complex interaction between different organs [5,6]. Adipose tissue is comprised of two major types lipid-storing white fat depots (e.g. visceral and subcutaneous (inguinal depots) and brown fat, which dissipates energy in the form of heat (thermogenesis) [7,8]. Thermogenic adipocytes (thermocytes) of different embryonic origins reside in different locations: brown adipose tissue or interspersed in white adipose tissue [9,10]. These thermocytes are called 'brown in white', 'brite', 'beige', or multilocular cells [11]. Independent of their origin, thermocytes express uncoupling protein 1 (Ucp1), which can increase daily energy expenditure by up to 20% in humans [12].

Visceral fat is a fundamental and integral component of obesity. Visceral fat secretes cytokines that provoke insulin resistance and

* Corresponding author. 1787 Neil Avenue, 331A Campbell Hall, Columbus, OH 43210, USA. Tel.: +1 614 292 5034; fax: +1 614 292 8880.
E-mail address: ziouzenkova.1@osu.edu (O. Ziouzenkova).
[1] These laboratories contributed equally to this work.

0142-9612/$ – see front matter © 2012 Elsevier Ltd. All rights reserved.
doi:10.1016/j.biomaterials.2012.04.035

chronic inflammation [13,14], which double the risk of cancer, cardiovascular diseases, and premature death from all causes [15–20]. In contrast, the progressive loss of subcutaneous tissue noted with aging correlates with development of insulin resistance, and type 2 diabetes [14]. Current pharmacologic or dietary therapies aimed at the reduction of obesity do not discriminate between subcutaneous and visceral adipose depots and are ineffective, especially in aging and disabled patients. Another critical shortcoming of these approaches is the poor compliance of patients to these regimens with inevitable attrition of therapeutic efficacy even after invasive bariatric and liposuction/lipectomy [21,22]. In the absence of effective treatment, obesity rates are increasing in epidemic proportions worldwide with 65 million more obese adults expected in the US alone by the year 2030 [23].

In mouse models, several genes playing a critical role in development of obesity have been identified [2,6]. Traditionally appetite- and energy expenditure- regulating hormones like leptin were considered for obesity treatment [2], but failed due to the development of leptin resistant conditions in rodents [24] and humans [25] with general obesity. Microcapsules with gut K cells secreting leptin also showed promising results in leptin deficient ob/ob mice; however, the microcapsules lack a therapeutic effect on high-fat (HF) diet-induced obesity in wild-type C57Bl/6J (WT) [2]. Many genes regulating thermogenesis or thermocyte differentiation successfully offset obesity on regular diets consistent with their role in energy expenditure [9,26,27] in genetically-modified animals. These genetic modifications were less effective on animals fed obesogenic diets (reviewed in [5]). Effects of engrafted thermocytes or cells catabolizing lipids for studies on energy balance in obese mice on HF diets have not been reported. It is unclear whether encapsulation is a suitable technology for the transplantation of these cells.

In our previous studies, we found remarkable resistance to HF diet-induced visceral obesity in aldehyde dehydrogenase 1a1 deficient (*Aldh1a1*$^{-/-}$) mice [28]. In these mice, the altered balance in bioactive vitamin A metabolites production increases metabolic rate, expression of thermogenic genes, and body temperature [28]. Our study examined how AP_L material supports survival and function of *Aldh1a1*$^{-/-}$ fibroblasts engrafted into visceral fat.

2. Materials and methods

2.1. Chemicals and reagents

We purchased reagents from Sigma–Aldrich (St. Louis, MO), cell culture media from Invitrogen (Carlsbad, CA), antibodies from Cell Signaling Technology (Danvers, MA) for Gapdh, Atgl, Ucp1, and β-actin; from Abcam (Cambridge, MA) for GFP (monoclonal), and β-tubulin; from LI-COR Biosciences (Lincoln, Nebraska) for secondary antibodies. FITC-insulin and Alexa Fluor 488-labeled IgG were from Invitrogen.

2.2. Animals

All experimental protocols were approved by the Institutional Animal Care and Use Committee.

Aldh1a1$^{-/-}$ mice were provided by Dr. Duester (Sanford-Burnham Medical Research Institute). Their construction and characterization was described before [29]. The mechanisms responsible for resistance of *Aldh1a1*$^{-/-}$ mice to visceral obesity and an HF diet-induced obesity were reported previously in [28,30].

2.3. Animal studies and metabolic measurements

Study 1. Four (4 weeks old) C57BL/6J (WT) and six *Aldh1a1*$^{-/-}$ female mice were fed a high-fat diet (HF, 45% kcal from fat with standard vitamin A content, 4 IU/g, D12451, Research Diets Inc., New Brunswick, NJ) for 14 months. Visceral (peri-ovarian) subcutaneous (inguinal), and brown fat were collected at the end of the study for mRNA analysis and embedded into paraffin for histological examination (see 2.9).

Encapsulation study 2. Fifteen 3-month-old WT female mice were fed a high-fat diet for 90 days. Then mice were randomly assigned into three groups ($n = 5$ each):

1) injected with vehicle (1 mL sterile phosphate buffer (PBS),
2) injected with encapsulated ^{G}WT fibroblasts ($0.5*10^6$ cells in 1 mL PBS per visceral depot)
3) injected with encapsulated ^{G}KO fibroblasts ($0.5*10^6$ cells in 1 mL PBS per visceral depot).

Mice were injected with vehicle or encapsulated cells into both visceral (peri-ovarian) depots and maintained on a similar HF diet for 80d. Two weeks prior to the end of the study, metabolic parameters in the treated mice were measured by indirect calorimetry (CLAMS, Columbus Instruments, Columbus, OH) at ambient temperature (22 °C) with 12 h light/dark cycles. Animals were fed the same HF diet and water provided *ad libitum*. Mice were placed individually and allowed to acclimatize in the chambers for 12 h, and O_2 consumption, CO_2 production, energy expenditure, and locomotor activity were measured for 24 h. Based on these data, respiratory quotient or exchange ratio (V_{CO2}/V_{O2}) and Δ heat values were calculated by CLAMS. Metabolic rate (MR) was calculated based on Romijn and Lokhorst formula as described previously [31]: $MR = 16.18*V_{O2}+5.02*V_{CO2}$. For glucose tolerance tests (GTT) mice were fasted overnight and were injected with a single intraperitoneal 25% glucose dose (0.004 mL/g body weight). Blood glucose was measured by One Touch Ultra Glucometer (LifeScan).

2.4. Magnetic resonance imaging (MRI)

At the end of the study 2, body fat was measured by 9.4T Bruker BioSpin wide-bore scanner as described before [30]. Multi Slice Multi Echo sequence (repetition time 1400 ms; echo time 12 ms; flip angle 180°; matrix 128 × 128; 4 averages) was used to acquire a total of 80 1-mm-thick images per mouse scanning from the tail to the head. ParaVision 4.0 software was used for MR acquisition and reconstruction. All image processing and analysis was performed in OsiriX software (The Osirix Foundation, Geneva, Switzerland).

2.5. Organ collection, lipid extraction, and western blot analysis

After MRI mice were anesthetized, blood was collected by cardiac puncture. EDTA plasma was prepared by centrifugation. Plasma was analyzed for non-esterified fatty acids (NEFA) using colorimetric assay (Wako Diagnostics, Richmond, USA). One whole subcutaneous and visceral (peri-ovarian) fat pads were dissected and homogenized in RIPA buffer with protease inhibitors. Aliquots from fat pad homogenates were used for lipid extraction, protein (Bicinchoninic Acid Kit) measurements, and western blots. Lipids (total lipophilic compounds) were extracted from 100 μL RIPA buffer using first, 10 μL ethanol, and then 700 μL hexane and 50 μL chloroform. After 1 min vortexing and centrifugation (4000 rpm), the organic phase was collected and dried under N_2. For Western blot analyses, tissue lysates were separated on 10% acrylamide gel under reducing conditions. After transfer to a polyvinylidene fluoride membrane (Immobilon-P, Millipore), proteins were analyzed using an Odyssey Infrared Imaging System (LI-COR). Images were quantified by ImageJ software.

2.6. Immunohistochemistry

The remaining fat pads were embedded in paraffin and in OCT for immunohistochemical analysis and laser microdissection. Sections (14 μm) were stained with hematoxylin and eosin (H&E) using a modified hematoxylin QS procedure [32] followed by dehydration in graded alcohol [33] or with Ucp1 polyclonal rabbit antibodies (both 1:1000 dilution).

2.7. Encapsulation

The phase microencapsulation technique for preparation of alginate-poly-L-lysine (AP_L) microcapsules has been performed as described [34]. The cell suspension (2×10^6 cells/ml) were suspended in 2% sodium alginate solution (Sigma, St. Louis, MO, MW 12,000–80,000 g/mol, 100–300 cps Brookfield viscosity). Then, this suspension was extruded through a inner diameter of 0.337-mm needle (23 gauge) into a 100 mM $CaCl_2$ solution, using Encapsulation Unit (Nisco Engineering AG, Switzerland) at 5.4 kV to form calcium alginate gel beads. Nozzle size, flow rate, and vibration frequency were identical for all encapsulation experiments. The gel beads trapped with cells were solidified in 100 mM $CaCl_2$ for 20 min, and then incubated with 0.05% (w/v) poly-L-lysine (MW 20,700, Sigma, St. Louis, MO) to form alginate-poly-L-lysine membrane around the surface. The membrane-enclosed gel beads were further suspended in 50 mM sodium citrate to liquefy the alginate core. Encapsulated fibroblasts were cultured with floating status in standard medium instead of embedding at the sodium alginate gel within the microcapsule and were maintained in culture under standard conditions for up to 30d.

2.8. Cell line engineering

Embryos (16 days-old) were collected from C56/BL6 (WT) and *Aldh1a1*$^{-/-}$ mice. WT and *Aldh1a1*$^{-/-}$ fibroblast cell lines were derived from embryonic fibroblasts and immortalized by following a classical protocol by Green & Meuth [35]. Then, WT and *Aldh1a1*$^{-/-}$ fibroblasts were transfected with PReceiver-Lv08GFP (Lentigen)

suspension (25 MOI/10^4 cells) in the presence of Polybrene (Millipore) transduction reagent in serum-free MEM-medium. After 3 h, cells were supplemented with 10% heat inactivated calf serum. Stable clones were selected with puromycin (0.75–1.5 mg/mL, Invitrogen). Single transfected cells were selected to derive GFP-labeled fibroblast lines ^{G}WT and ^{G}*Aldh1a1*$^{-/-}$ (defined as ^{G}KO).

2.9. Cell differentiation

Fibroblasts ^{G}WT, ^{G}KO, and 3T3-L1 were cultured in DMEM medium containing 10% calf serum. Differentiation medium contained 10% FBS, 10 μg/mL insulin, 1 μM dexamethasone, 0.5 mM 3-isobutyl-1-methyl xanthine. Medium was replaced every 48 h with DMEM containing 10% FBS, 10 μg/mL insulin, and continued for 7 days.

2.10. mRNA analysis

mRNA was purified from adipocytes or adipose tissue according to the manufacturer's instructions (Qiagen) and quantified using 7900HT Fast Real-Time PCR System and TaqMan fluorogenic detection system (Applied Biosystems). Validated primers were also purchased from Applied Biosystems. Comparative real-time PCR was performed in triplicate, including no-template controls. Expression was calculated using the comparative Ct method normalized to 18S.

2.11. Laser microdissection pressure catapulting (LMPC)

Frozen H&E sections were mounted on each RNAZap and UV-treated thermoplastic (polyethylene napthalate)-covered glass slide (PALM Technologies, Bernreid, Germany) and kept at −80°C until use. LMPC was performed by using the laser microdissection system from PALM Technologies (Carl Zeiss MicroImaging GmbH, Germany) containing a PALM MicroBeam and RoboStage for high-throughput sample collection and a PALM RoboMover (PALM Robo software, version 4.2) as described [32,33,36]. Approximately 250,000 μm^2 of tissue area of both capsule and host tissue were captured under 10× objective. Typical settings used for laser cutting were UV energy of 56–65 and UV focus of 80 was used [36]. Cut elements were catapulted into 25 μl of extraction buffer from the PicoPure RNA Isolation Kit, (Arcturus) as described [36] and stored at −80°C. Total RNA was isolated using PicoPure RNA Isolation Kit (Arcturus) [36]. RNA was first measured for quality using the NanoDrop system (NanoDrop Technologies, Wilmington, DE) and Bioanalyzer (Agilent Technologies, Santa Clara, CA). LPMC captured RNA were subjected to reverse transcription using SuperScript VILO cDNA synthesis kit (Invitrogen, Carlsbad, CA) and quantified using TaqMan PCR kit as described above.

2.12. Statistical analysis

Data are shown as mean ± SD of experiments that were performed at least with $n = 3$ in vitro and $n = 5$ in vivo. Group comparisons were performed using non-parametric Mann–Whitney *U* test unless otherwise indicated.

3. Results

3.1. Characteristics of cells selected for APL encapsulation

Aldh1a1$^{-/-}$ mice, which have been previously characterized as resistant to an HF-diet –induced obesity, visceral fat accumulation, and their high metabolic rate, were considered as candidate donor cells for encapsulation [28,30]. To clarify whether *Aldh1a1* deficiency stimulates energy dissipation in the visceral fat depot, we fed WT and *Aldh1a1*$^{-/-}$ female mice an HF diet for 14 months. Similarly to our previous studies [28,30], *Aldh1a1*$^{-/-}$ mice weighed significantly less than the WT group. These differences were even more pronounced by comparison of weight gain between these mice groups (Fig. 1a). *Aldh1a1* deficiency did not influence the brown fat mass but prevented fat accumulation in the visceral and subcutaneous fat tissue in *Aldh1a1*$^{-/-}$ compared to WT mice (Fig. 1b).

The mRNA expression in the *Aldh1a1*$^{-/-}$ *vs*. WT visceral fat revealed similar levels of fatty acid binding protein (*Fabp4*) and brown adipocyte marker *Prdm16*, but higher levels of mitochondrial cytochrome oxidase IV isoform 1 enzyme (*Cox4i1*), peroxisome proliferator activated receptor gamma coactivator 1α (*Pgc1α*), and thermogenic *Ucp1* (Fig. 1c). Protein levels of Ucp1 also were 572% higher in visceral fat of *Aldh1a1*$^{-/-}$ than WT mice (Fig. 1d). Histological staining of Ucp1 protein expression in visceral fat shows large numbers of multilocular Ucp1-positive cells that were interspersed in white adipose tissue and also formed clusters (Fig. 1e). Brown fat (Fig. 1d, western blot insert) comprising of multilocular thermogenic adipocytes had higher Ucp1 protein levels than *Aldh1a1*$^{-/-}$ visceral fat. Combined, these data suggest that gene and protein expression in *Aldh1a1*$^{-/-}$ visceral adipocytes support moderately-elevated thermogenic energy dissipation in these cells.

Next, we tested whether isolated *Aldh1a1*-deficient fibroblast maintain higher thermogenic gene expression in vitro. WT and *Aldh1a1*$^{-/-}$ embryonic fibroblasts were immortalized and then stably transfected with green-fluorescent protein (GFP) to establish heritably labeled cell lines (^{G}WT and ^{G}KO, respectively). Compared to ^{G}WT, ^{G}KO expressed similar levels of *Fabp4* and *Ucp3*, but higher levels of *Cox4i1*, *Pgc1α*, and *Ucp1* (Fig. 1, f). Overall, ^{G}KO fibroblasts after adipogenic differentiation in vitro replicate thermogenic gene expression seen in *Aldh1a1*$^{-/-}$ visceral fat in vivo.

3.2. AP_L microcapsule characteristics

AP_L microencapsulation has been characterized previously [34]. We tested each microcapsule batch for permeability and biocompatibility using fluorescein isothiocyanate (FITC)- or Alexa Fluor 488-labeled (AF488) proteins with different molecular weights. A diffusion of FITC-insulin (~6.5kD) from microcapsules into external PBS has reached the equilibrium in less than 5 min (Fig. 2, a), demonstrating the permeability of microcapsule for insulin. In contrast, mouse immunoglobulins (AF488-IgG, 32kD) were not able to influx into microcapsules from the external PBS, verifying known permeability of AP_L microcapsules [34] (Fig. 2, b). This procedure was then used to enclose approximately 500 ^{G}WT or ^{G}KO in microcapsules (Fig. 2, c). Encapsulated cells were maintained in culture for up to 3 weeks.

3.3. Interaction of encapsulated fibroblasts with adipocytes in vitro

To examine interactions between adipocytes and encapsulated ^{G}WT and ^{G}KO cells, we co-incubated ^{G}WT and ^{G}KO microcapsules on a layer of mature NIH3T3-L1 adipocytes. The co-incubation with microcapsules influenced triglyceride content in mature NIH3T3-L1 adipocytes (Fig. 2, d). Empty (acellular) and encapsulated ^{G}WT fibroblasts stimulated triglyceride accumulation in NIH3T3-L1 adipocytes (139% and 134% compared to 100% in non-treated adipocytes) due to the 3D microevironment created by microcapsules' surfaces [37]. In contrast, co-incubation of these adipocytes with ^{G}KO microcapsules decreased triglyceride content in NIH3T3-L1 adipocytes by 61.6% compared to that seen in adipocytes treated with empty capsules. Thus, encapsulated ^{G}KO cells were capable of lowering lipid content of their surrounding cellular milieu. In a subsequent systematic study, we examined in vivo interaction between ^{G}WT and ^{G}KO microcapsules and host adipocyte tissue.

3.4. Biocompatibility and MRI of encapsulated cell engrafts in visceral fat

Fifteen WT female mice were kept on an HF diet for 90 days prior to the treatment with microcapsules to induce obesity. Mice were assigned to three treatment groups: 1) no treatment, 2) treatment with ^{G}WT microcapsules and 3) treatment with ^{G}KO microcapsules. Mice were injected with vehicle, or encapsulated cells into both perigonadal visceral depots. After the single injection, all mouse groups continued on HF diet for 80 days. To spatially locate injected microcapsules, we performed whole-body magnetic resonance imaging (MRI) of non-treated and treated with ^{G}WT and ^{G}KO microcapsules animals at the end of study (Fig. 3, a). T1-weighted

axial MRI scans in mice treated with microcapsules showed well-defined elliptical structures in the reconstructed coronal views (Fig. 3, a, insert) which differed in their signal to noise ratio (SNR) compared to surrounding fat and muscle (Fig. 3, b). The low signal was likely a consequence of long T1 relaxation times of the capsule interior. 3D MR image reconstruction revealed the location of multiple microcapsules in the visceral fat (Fig. 3, a, lower insert & suppl. video). Notably, no microcapsules were seen either in the

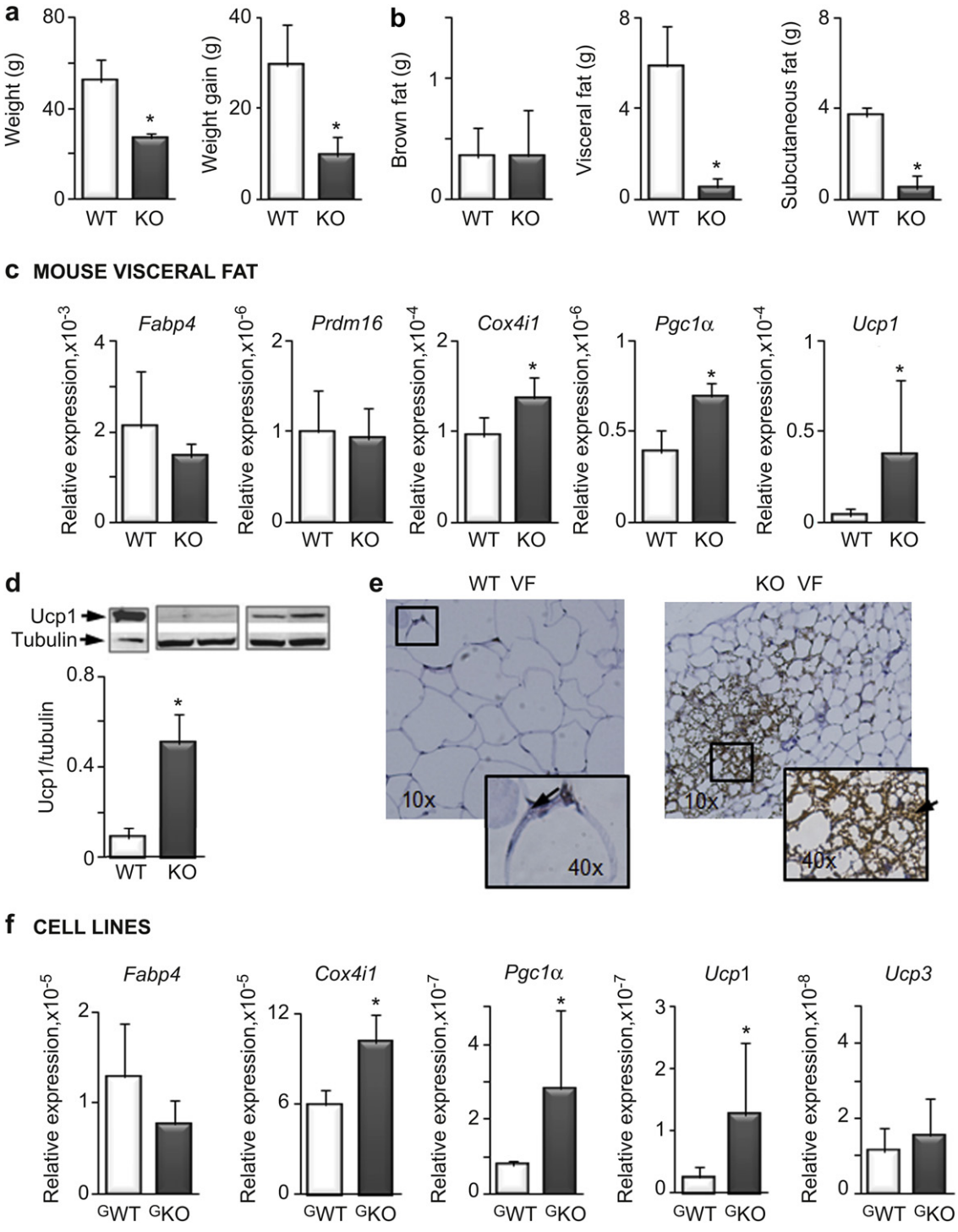

Fig. 1. (a) Reduced weight and weight gain in *Aldh1a1*$^{-/-}$ (KO) vs. WT mice that were fed HF diet for 14 months (Study 1). Here and throughout this figure: *, Asterisk, – significant differences between WT and KO adipocytes ($P < 0.05$, Mann-Whitney *U* test). (b) Similar weight of brown fat pads, but significantly reduced weight in white fat depots, visceral (peri-ovarian) and subcutaneous (inguinal) in KO *vs*. WT mice from same study. (c) mRNA expression of *Fabp4*,*Prdm16, Cox4i1*, *Pgc1α*, and *Ucp1* in visceral fat of WT and KO mice was measured by TaqMan. (c) Ucp1 protein levels in visceral fat of KO and WT mice were measured by western blot (all $n = 4$, mean ± SD). Protein levels were normalized to β-tubulin for quantification. Insert (above) showed one representative western blot comparing Ucp1 protein levels in WT brown fat with visceral fat isolated from WT and KO mice. (e) Representative Ucp1 staining (brown staining, examples of Ucp1 staining are indicated by arrows) of paraffin embedded visceral fat from WT and KO mouse groups at 10×. Selected areas with Ucp1-positive staining are shown at 40× magnification. (f) mRNA expression of *Fabp4*, *Cox4i1*, *Pgc1α*,*Ucp1*, and *Ucp3* was measured by TaqMan in KO and WT fibroblasts cell lines stably transfected with GFP (^{G}KO, ^{G}WT). Fibroblasts were differentiated for 7 d after stimulation with adipogenesis-inducing hormone mix. Data are shown as mean ± SD ($n = 3$). *, – significant differences between ^{G}WT and ^{G}KO adipocytes ($P < 0.05$, Mann-Whitney *U* test).

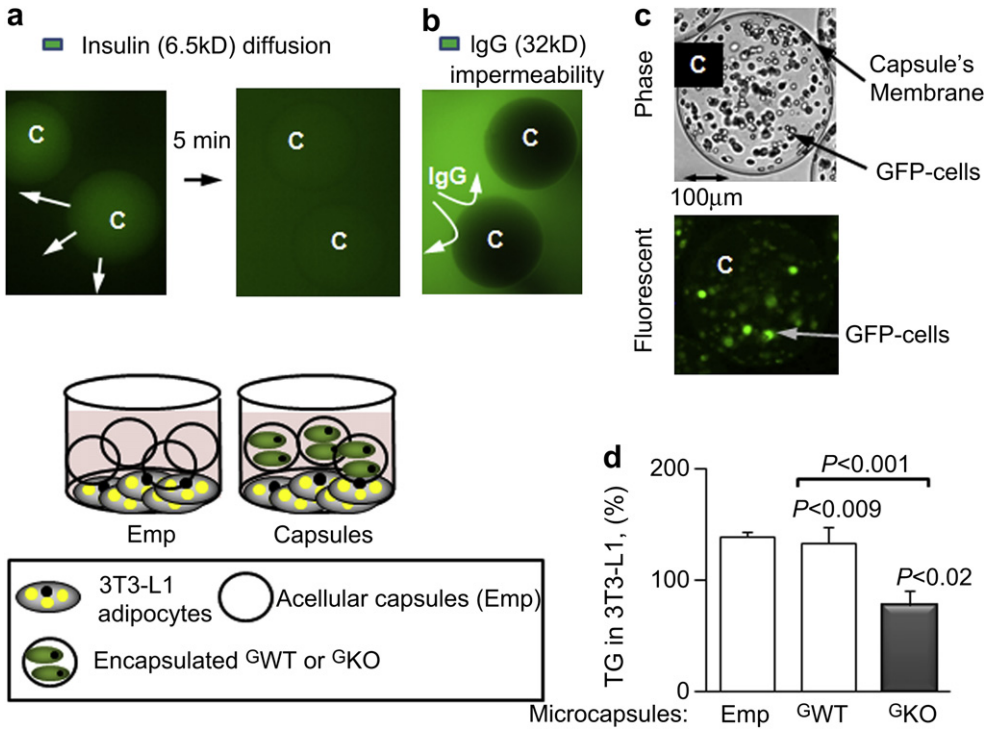

Fig. 2. (a) Rapid diffusion (1–5 min) of FITC-labeled insulin (~6.5kD) from the microcapsules. Microcapsules containing recombinant FITC-insulin were immersed into PBS. The rapid diffusion was followed by green fluorescence under the microscope. White C, microcapsules. Arrows indicate efflux of FITC-insulin representing low molecular weight molecules. (b) The lack of influx of Alexa Fluor 488 (AF488)-labeled IgG (32kD) into microcapsules. Arrows indicate impermeability of microcapsules for AF488-IgG and other molecules (>30kD). Observation was continued for 15 min. (c) Light and fluorescent microscope images of ^{G}Th fibroblasts encapsulated using the phase microencapsulation technique (10×). There were approximately 500 cells per capsule. C, microcapsules. Arrow indicates a light reflection from capsule's alginate-poly-L-lysine (AP_L) membrane, which is invisible under other imaging conditions (under fluorescent microscope or histology sections). (d) 3T3-L1 fibroblasts were differentiated into mature adipocytes for 8 days. Then acellular (empty), ^{G}WT, or ^{G}KO-containing microcapsules were added to form a monolayer of 102 microcapsules/cm^2. Adipocytes were incubated with microcapsules for the additional 6 days. The experiment was performed in 6-well dishes. Adipocytes were harvested in RIPA buffer (100 μL) and analyzed for triglyceride (TG) and protein content to obtain a TG/protein ratio. Data (mean ± SD, $n = 3$ per condition) are shown as percent of TG/protein ratio in 3T3-L1 adipocytes, which were not treated with microcapsules (none, 100%) to those treated with different microcapsules. *P*, significance measured by Mann–Whitney *U* test.

subcutaneous fat depots of injected mice or inside non-injected animals.

Supplementary video related to this article can be found online at doi:10.1016/j.biomaterials.2012.04.035.

Histological examination of visceral fat also showed enclosed microcapsules containing GFP-positive ^{G}WT and ^{G}KO cells that were surrounded by host adipocytes only in the injected depot (Fig. 3, b). Microcapsules were approximately 8 times larger than the host visceral adipocytes. The whole capsule images (10×, Fig. 3, c insert) indicated that the center of microcapsules was empty because ^{G}WT and ^{G}KO fibroblasts were adherent to the inner surface of the capsule's membrane. This localization, probably, enables favorable exchange of small molecules among transplanted and host cells. Inside the microcapsules, ^{G}WT and ^{G}KO fibroblasts were adjacent to a basic protein membrane that was produced in vivo by cells. Empty core of microcapsules represent structures with low interior content resulting in a long T1 relaxation time and appearing dark on MR images.

Using histology slides for measurement of radius of microcapsules (~300 μm) and the cell numbers within the circumferential segments, we calculated the number of cells in the microcapsule assuming their spherical shape and equal cell distribution around surface. Each capsule contained approximately 22,000 cells that were indicative of limited cell proliferation as expected in fibroblasts capable of differentiation. Cells formed only 3-5 layers on the inner surface of the microcapsules. ^{G}WT and ^{G}KO fibroblasts in microcapsules were surrounded by adipocytes, suggesting that fibrosis and inflammation were not excessive for a prolonged (80 days) period of time. Unlike host adipocytes, ^{G}WT and ^{G}KO fibroblasts did not deposit lipids. Next, we studied whether the presence of viable encapsulated cells in visceral fat modulates obesity.

3.5. Effects of encapsulated cells on lipid accumulation in vivo

All mice had similar weight at the beginning of the study (Fig. 4a,'before'). After 80 d on the same HF diet, the mock- and ^{G}WT-injected mice gained weight (Fig. 4a, 'after'), whereas mice injected with ^{G}KO microcapsules had similar weights as those seen prior to injection (Fig. 4a, 'after', right panel). The kinetics of weight changes varied over the course of the study (Fig. 4b). Injection of the vehicle, ^{G}WT, or ^{G}KO microcapsules resulted in some weight loss in mice until day 2. After that, the control group steadily gained weight at a rate that was observed in all mice groups before injection. In contrast, mice injected with ^{G}WT, or ^{G}KO microcapsules, rapidly lost 11% and 15% of body weight seen in these groups prior to the injection. After 23 days, mice injected with ^{G}WT and ^{G}KO microcapsules began to gain weight. However, ^{G}KO - injected mice gained less weight than ^{G}WT group and maintained similar weight change as seen at the day of injection (Fig. 4b, dashed line) in spite of an HF diet consumption. To rule out that the initial weight loss is caused by microcapsule injection, we injected empty microcapsules into visceral fat in a pilot study (Fig. 4, b, insert). Empty capsules had no effect on HF diet-induced obesity, while obese mice injected with ^{G}KO microcapsules lost 10% of weight within the first week of the injection.

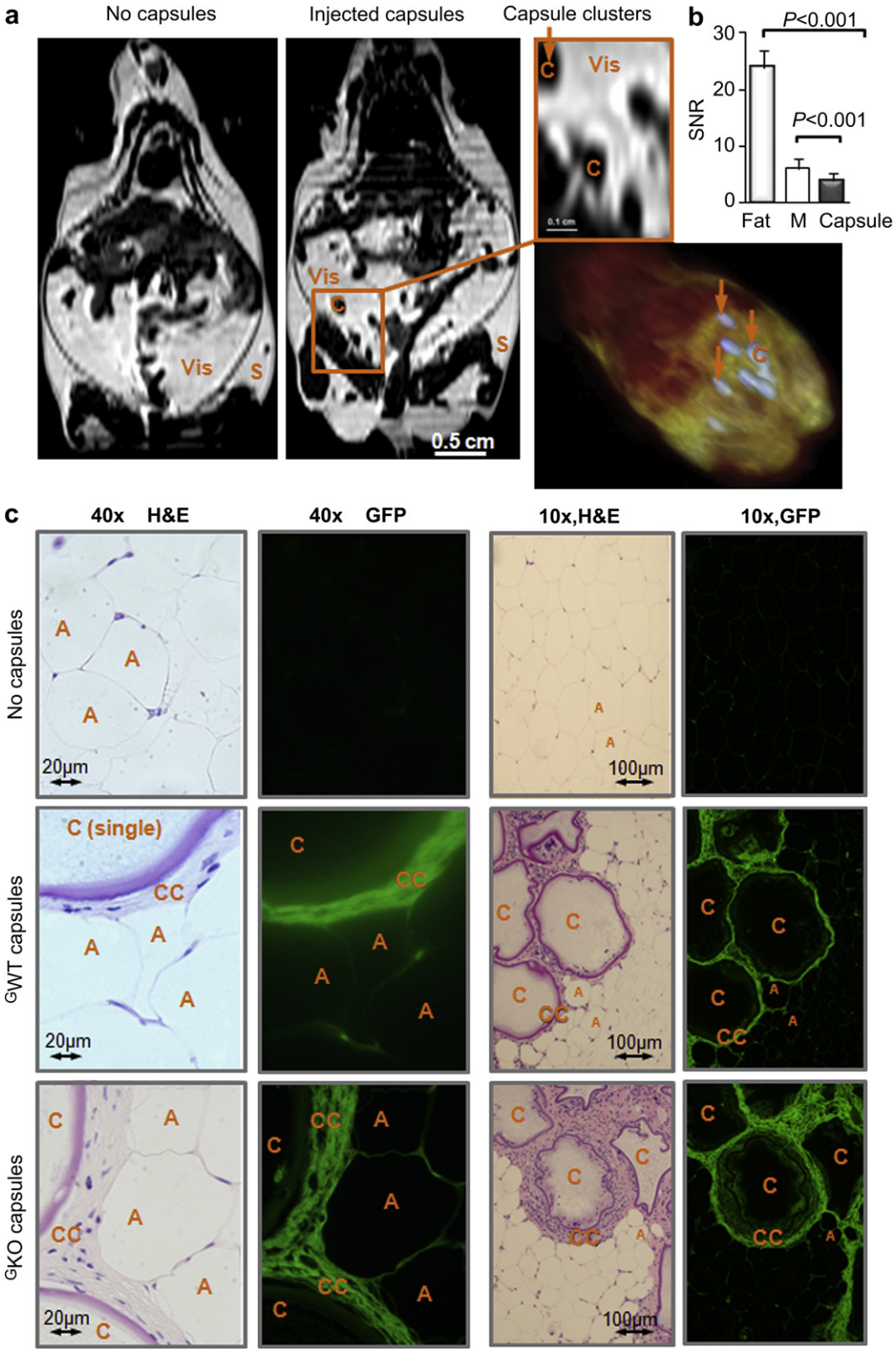

Fig. 3. (a) Representative magnetic resonance whole-body images from a control (injected with PBS) and treated (injected with either ^{G}WT or ^{G}KO microcapsules into visceral fat depot) mice were obtained using 9.4 T MRI scanner. Dark elliptical structures with long T1 relaxation time were identified as microcapsules (C, orange) when the signal to noise ratio (SNR) ratio was lower than in adipose (fat) and muscle tissues (M), indicating low proton density of microcapsules' interior (b). Insert shows 3D MR image reconstruction of identified microcapsules (C, blue) interspersed within visceral (vis), but not subcutaneous fat. Adipose and muscle tissues are shown in yellow and red, respectively (see 3D image in Suppl. video). (c) Representative sections of visceral fat isolated from control and injected with ^{G}WT and ^{G}KO capsule mice. Visceral fat was dissected 80 days after injection. Paraffin embedded sections were stained with hematoxylin&eosin (H&E) to visualize all cells in the adipose tissue. In the same slide GFP-labeling indicates implanted microcapsules (C), containing green encapsulated cells (CC), but not host adipocytes (A). The larger, 40×, magnification shows multiple engineered cells (CC) on the border of a capsule. Due to the fact that GFP-positive cells were equally spread and adherent to the inner side of APL polymer shell (invincible), the microcapsules were observed as circular fluorescent structures in the fluorescence images. Pink eosin staining indicated a protein matrix within the microcapsules that was not present in vitro (Fig. 2c). Lower, 10× magnification shows the whole capsule within the capsule's cluster. Host adipocytes were smaller in size than the microcapsules ('A' *vs.* 'C').

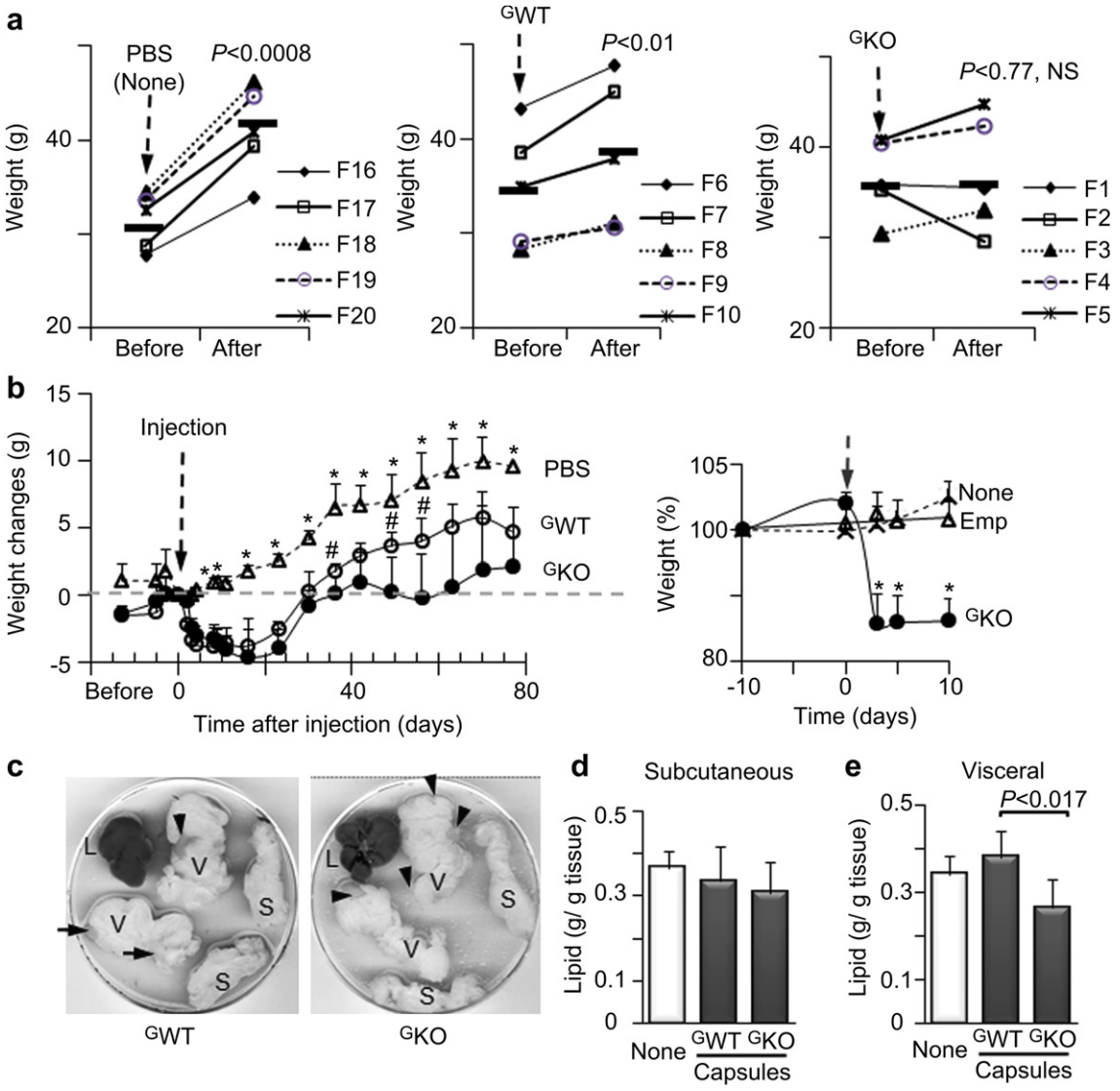

Fig. 4. (a) Weight of obese mice on an HF before injections with PBS (mock-injection), and microcapsules containing ^{G}WT and ^{G}KO fibroblasts and 80 days after injection (Study 2). Mice were C57BL/6J (WT), $n = 5$ per group. Symbols represent individual mice encoded with F (number), ▪ indicates weight average in each group. Mice were on an HF throughout the study. *P*, significance values determined by paired *t*-test. NS, not significant. (b) Kinetics of weight gain in a control mouse group injected with 1 mL PBS (open triangles) and weight loss in mice injected with ^{G}WT microcapsules (open circles) or ^{G}KO microcapsules (closed circles). Black dashed line indicates the time of injection. Gray dashed line shows the weight on a day of injection. Data are shown as mean ± SD with five animals per group, significance levels ($P < 0.05$) were measured by Mann–Whitney *U* test.*, significant differences between the control and mouse groups treated with encapsulated cells. #, significant differences between mice injected with ^{G}WT and ^{G}KO microcapsules. Insert shows weight change in the non-treated obese mice (dashed line), and mice treated with acellular (emp, triangles) and ^{G}KO microcapsules (solid circles) in a pilot group of 9 female WT obese mice fed HF diet throughout study. Mice were injected with ^{G}KO or acellular (empty) microcapsules (Both groups: $4*10^5$ in 0.5 mL PBS, $n = 3$, mean ± SD). The remaining mouse group was not injected (not treated, $n = 3$). Injection time is indicated by an arrow. Food consumption was similar in all mice before and after injection, while weight was reduced only in mice injected with ^{G}KO. Data are shown as mean ± SD. Weight change (%) was compared to weight of each mouse10 days prior to injection (100%). *, significant differences between the control and mouse groups treated with encapsulated cells. (c) Representative visceral (V) and subcutaneous (S) fat pads and liver (L) from Study 2. Organs were collected after dissection into P100 dishes. Arrow shows visible clusters of microcapsules that appeared at different amounts and locations on visceral fat pads. (d & e) Lipid weight per gram of subcutaneous (d) or visceral (e) fat pad dissected from mice from Study 2. One whole fat pad from each mouse was weighed, and, then, homogenized in equal volume of RIPA buffer. Lipids weights were determined after homogenate extraction and evaporation of organic phase under nitrogen gas. Protein content was also measured in the remaining homogenate to obtain lipid per gram protein ratio.

We next examined if weight changes resulted from the altered lipid metabolism in visceral fat. After dissection visceral fat pads have visible clusters of microcapsules (Fig. 4c, some of grey clusters were indicated by arrows), which contribute to the weight of these depots. Therefore, we quantified total lipid content in visceral and subcutaneous fat depots using lipids extracted from whole homogenized subcutaneous and visceral fat pad in each animal. The lipid contents in non-injected subcutaneous fat were similar in mice injected with the vehicle or encapsulated cells (Fig. 4d). In contrast, lipid content of visceral fat depots was significantly 31% lower in ^{G}KO - compared to ^{G}WT-injected group (Fig. 4e). Of note, the most potent anti-obesity drug Qnexa reduced approximately 10% of total body weight [38].

To account for contribution of encapsulated cells to the protein in the injected depots, we measured GFP levels in same homogenates (Fig. 5a). Samples were normalized to ponceu red, because the levels of housekeeping genes (actin, tubulin, Gapdh) were different in the encapsulated cells and host adipocytes. Even though mice were injected with the similar number of cells, we found dissimilar GFP levels in the visceral fat, suggesting different

numbers of the transplanted cells at the end of study. Lipid content in visceral depots was inversely correlated with the GFP portion of protein (Fig. 5b), suggesting participation of encapsulated cells in visceral fat catabolism.

3.6. Interaction of encapsulated cells and host adipocytes

To gain insight into mechanisms of interactions between encapsulated cells and host adipose tissue, we employed laser microdissection and pressure catapulting (LMPC) as well as immunohisto chemistry analyses. Strikingly, protein levels of adipose triglyceride lipase (Atgl), the major triglyceride lipase in the adipose tissue, was higher in the control visceral fat compared to that treated with encapsulated cells (Fig. 5a,c); however, this traditional analysis does not provide information about differences in Atgl levels in engrafts and host tissue. We developed LMPC procedure to isolate encapsulated cells from the adjacent host adipocytes from histological sections (Fig. 5d). The captured encapsulated cells and host tissue were analyzed for mRNA quality (Fig. 5e), and the expression of selected abundant genes, such as Atgl. *Atgl* expression levels in the encapsulated ^{G}WT and ^{G}KO fibroblasts were lower compared to the host tissue (Fig. 5f), suggesting that transcriptional activation of this lipolytic enzyme occurs primarily in the host tissue.

In contrast, higher Ucp1 protein levels were found in the visceral fat treated with ^{G}KO microcapsules (Figs. 5a and 6a). The visceral fat pads injected with ^{G}KO microcapsules had 208% higher Ucp1 protein levels compared to the control mice, whereas the moderately higher Ucp1 levels in ^{G}WT-treated mice were elevated, but not

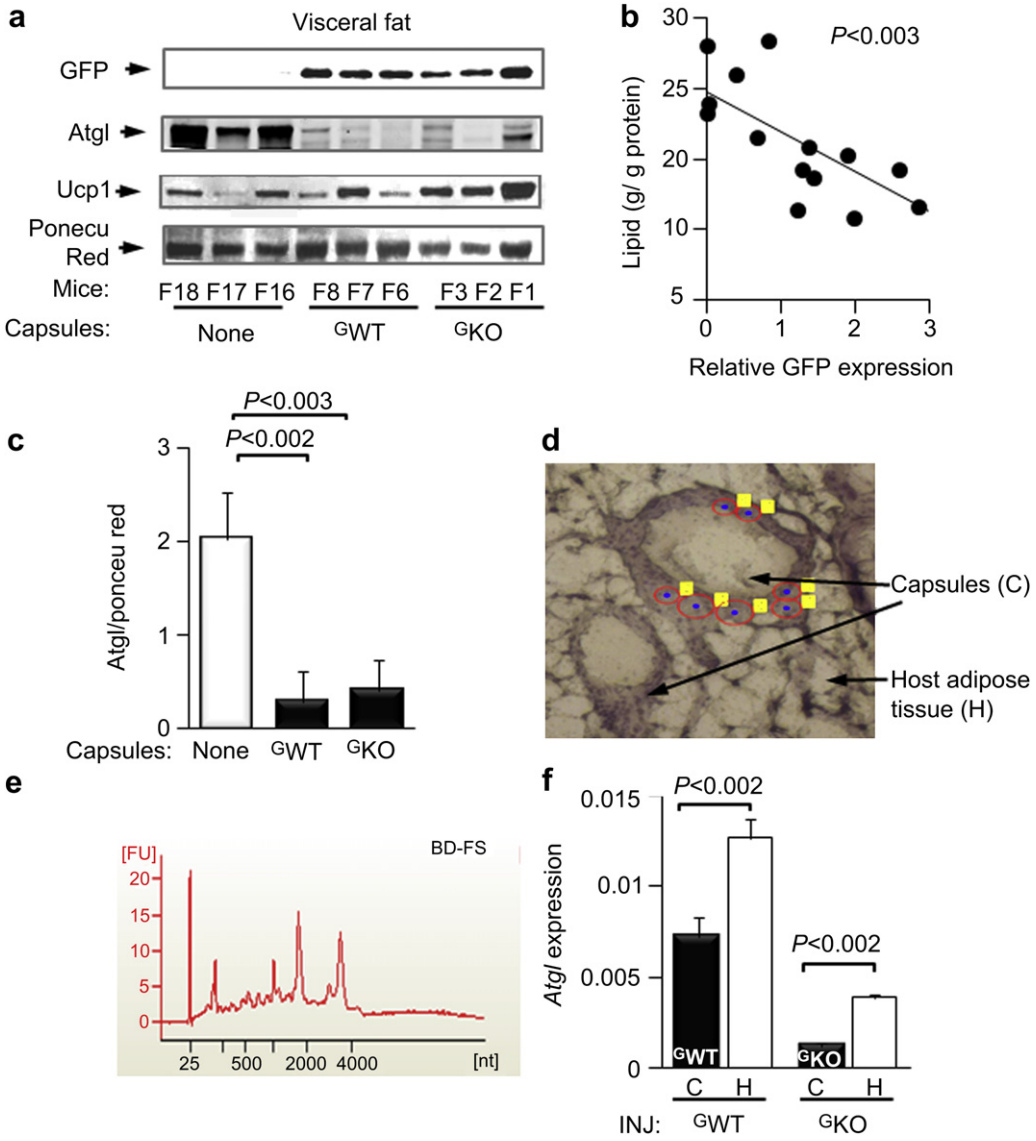

Fig. 5. (a) One representative western blot of protein homogenates ($n = 3$ per group, F, codes of mice used for this experiment. same as used in Fig. 4e) from whole visceral fat pads that were analyzed for GFP, Atgl, and Ucp1 protein content. Data were normalized by ponceu red staining due to the dissimilar concentrations of housekeeping genes in the microcapsules and host tissue. Quantified data from all 5 mice per group are shown in Figs. 5e and 6a. (b) Inverse correlation between GFP content and lipid per protein ratio in visceral fat from control and treated mice groups. *P*, significance levels were measured by *ANOVA*. (c) Protein homogenates ($n = 5$ per group, same as used in Fig. 5a) from whole visceral fat pads were analyzed for Atgl protein content by western blot and normalized by ponceu red staining. *P*, significant difference were determined by Mann-Whitney *U* test. (d) Selected area for laser microdissection pressure catapulting (LMPC) capture (blue dots and red circles) indicates encapsulated cells ('C') within H&E stained frozen section from visceral fat. The identity of encapsulated cells was confirmed by green fluorescence. After collection of encapsulated cells the remaining host visceral adipose tissues ('H') were collected. (e) Representative electropherogram shows RNA quality that was performed in all extracted by LMPC samples. Samples with RNA integrity number values above 5 were used for mRNA expression measurements. (f) Atgl mRNA expression in capsulated cells ('C') and surrounding host visceral adipose tissue ('H') after LPMC dissection. Data was quantified using TaqMan assay. Samples (mean ± SD) were measured in triplicate and normalized by 18S expression. P, significance measured by Mann–Whitney *U* test.

significantly different from the control group (Fig. 6a). Moreover, while Ucp1 and GFP protein levels were not correlated in ^{G}WT-treated mice (Fig. 6b), Ucp1 and GFP protein levels significantly correlated in the visceral fat of ^{G}KO-treated mice (Fig. 6c). This correlation can suggest Ucp1 association with transplanted ^{G}KO fibroblasts. Ucp1 protein levels in this group were also inversely correlated with the lipid content of visceral fat (Fig. 6d), highlighting possible functional role of Ucp1 in the lipid content reduction.

An evidence of Ucp1 association with transplanted ^{G}KO fibroblasts was obtained from immunohistological staining in visceral fat injected with ^{G}WT *vs.* ^{G}KO microcapsules (Fig. 6e). As expected, Ucp1 protein was expressed in ^{G}KO, but not in ^{G}WT microcapsules in vivo. A surprising finding in our study was the markedly increased levels of Ucp1-positive cells in the host visceral fat (Fig. 6e, right panel), that occurred in clusters similar to those seen in the visceral fat of *Aldh1a1*$^{-/-}$ mice (Fig. 1e).

3.7. Effects of encapsulated cells on systemic energy balance

Metabolic monitoring revealed that the ^{G}KO-treated mice had higher heat production than those treated with ^{G}WT microcapsules. The differences in heat production between these mice groups were statistically significant at several time points (Fig. 7a). The respiratory quotient was comparatively lower in mice treated with ^{G}KO than ^{G}WT microcapsules, indicating a tendency to lipid consumption (Fig. 7b). Metabolic rate was moderately higher in mice injected with ^{G}KO compared to ^{G}WT microcapsules (Fig. 7c). The movement activity and food intake were not statistically different in ^{G}WT and ^{G}KO-treated groups (Fig. 5d, e). Glucose tolerance test indicated the trend to improved glucose metabolism in both ^{G}WT and ^{G}KO-treated groups; however, this trend reached statistical significance only at 15 and 30 min after injection (Fig. 7f).

4. Discussion

Our study applied AP$_L$ for encapsulation of cells with elevated lipid catabolism for treatment of obesity. We demonstrated the feasibility of implantation of AP$_L$-encapsulated ^{G}KO cells into visceral fat without pronounced immune response and fibrosis, in vivo detection of encapsulated cells by MRI, and functional reduction of lipids in the injected visceral, but not in non-treated subcutaneous depots. Depot-specific lipid reduction in visceral fat was attributed to the increased Ucp1 levels in the encapsulated cells and host tissue that facilitated energy dissipation. An impending implication of AP$_L$-encapsulated ^{G}KO cells is their therapeutic potential in reduction of desirable fat depots.

Encapsulated engineered cells have been used throughout the last two decades for the production of various bioactive peptides, tissue engineering, and wound dressing [1,3,4,39]. In these applications, AP$_L$ is the most frequently employed polymer, which was

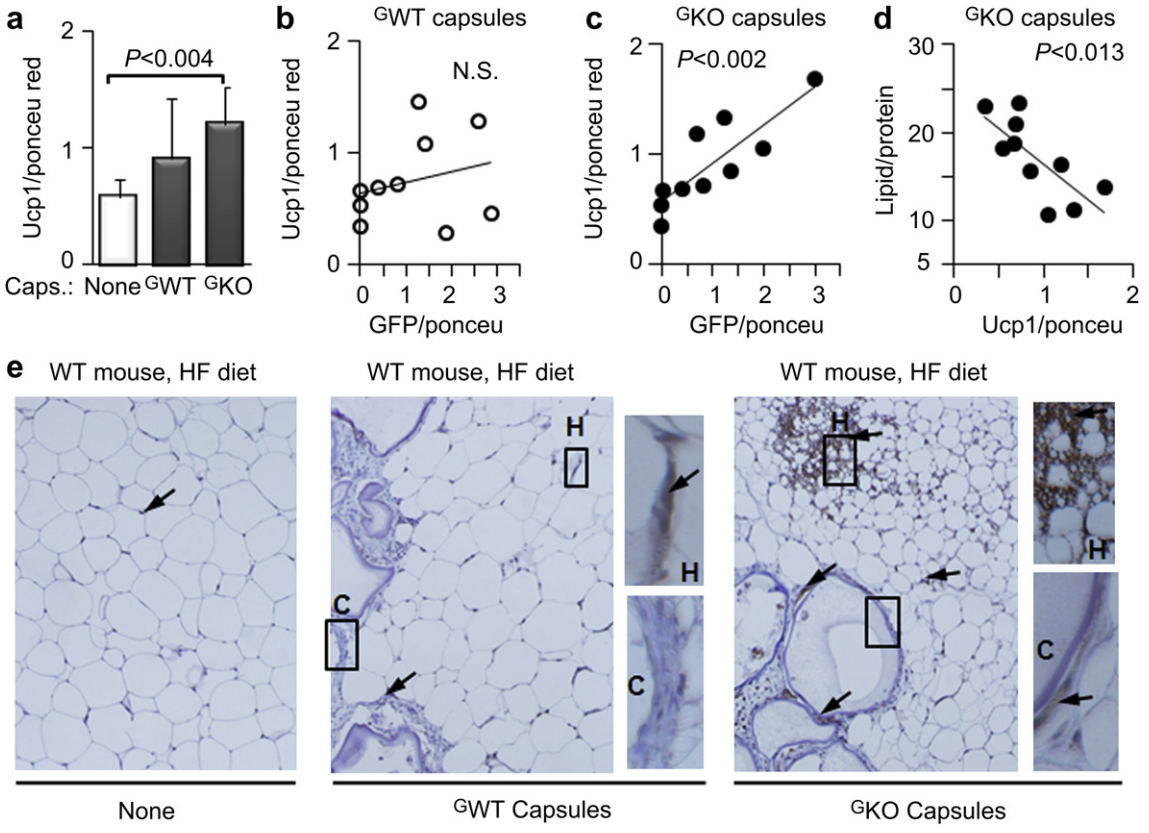

Fig. 6. (a) Protein homogenates ($n = 5$ per group, same as used in Fig. 5a) from whole visceral fat pads were analyzed for Ucp1 protein content by western blot and normalized by ponceu red staining. (b) Lack of a correlation between Ucp1 and GFP protein levels in visceral fat pads isolated from the control and ^{G}WT-treated mice. N.S., not significant, *ANOVA*. (c) Positive correlation between Ucp1 and GFP protein levels in visceral fat pads isolated from the control and ^{G}KO-treated mice. Significance levels were determined using one way *ANOVA*. (d) Inverse correlation between Ucp1 protein levels and lipid content (g lipid/g protein) in visceral fat pads isolated from the control and ^{G}KO- treated mice. Significance levels were determined using one way *ANOVA*. (e) Representative Ucp1 staining (brown, examples of Ucp1 staining are indicated by arrows) of paraffin embedded visceral fat from mock-injected, ^{G}WT- and ^{G}KO microcapsules injected mice at 10× magnification. Microcapsules indicated by 'C', the areas of host tissues as 'H'. Selected Ucp1-positive areas of microcapsules and host adipocytes are shown in at 40× magnification. Numerous Ucp1-positive clusters of cells were seen only in ^{G}KO-capsule injected areas. The identity of encapsulated cells was confirmed by green fluorescence (data not shown).

held responsible for adverse fibrosis and inflammation [40]. Here we implemented a reverse strategy by engineering 'consuming cells' capable of dissipating 'lipid energy' in the form of heat. The AP_L encapsulation of ^{G}WT and ^{G}KO fibroblasts in visceral fat substantially altered responses in host tissues and implanted cells compared to those reported previously [40]:

1) ^{G}WT and ^{G}KO fibroblasts were localized in the inner surface of the capsule's membrane, probably to enable exchange of metabolites with the host tissue.
2) ^{G}WT and ^{G}KO fibroblasts were not proliferating given their ability to differentiate into adipocytes in the presence of adipogenic hormones [30].
3) Intact ^{G}WT and ^{G}KO fibroblast-containing microcapsules were surrounded by host adipocytes suggesting limited fibrosis and inflammation after 80d implantation period. This effect could depend on the suppressed immune response of the host adipose tissue and/or on the low growth factor levels of ^{G}WT and ^{G}KO fibroblasts. More studies on microcapsules' composition after in vivo transplantation are needed to shed light on these phenomena.

We developed a laser capture microdissection (LMPC) method that permitted the dissection of encapsulated cells from AP_L materials and host adipocytes. Due to the limited amount of cell material, we quantitatively analyzed expression of abundant genes and attributed Atgl-mediated hydrolysis of triglycerides to the host adipose tissue. In the future, LPMC could reveal molecular pathways underlying interactions between AP_L-encapsulated cells and host tissue. Perimembranous localization of cells helped to solve a problem of non-invasive detection of encapsulated microcapsules in vivo. The MRI detects the low SNR of the empty microcapsules' core. The computer reconstruction provided the 3D position of microcapsules in the fat tissue. The exact location of encapsulated cells is important for translation of microencapsulation applications for future therapies.

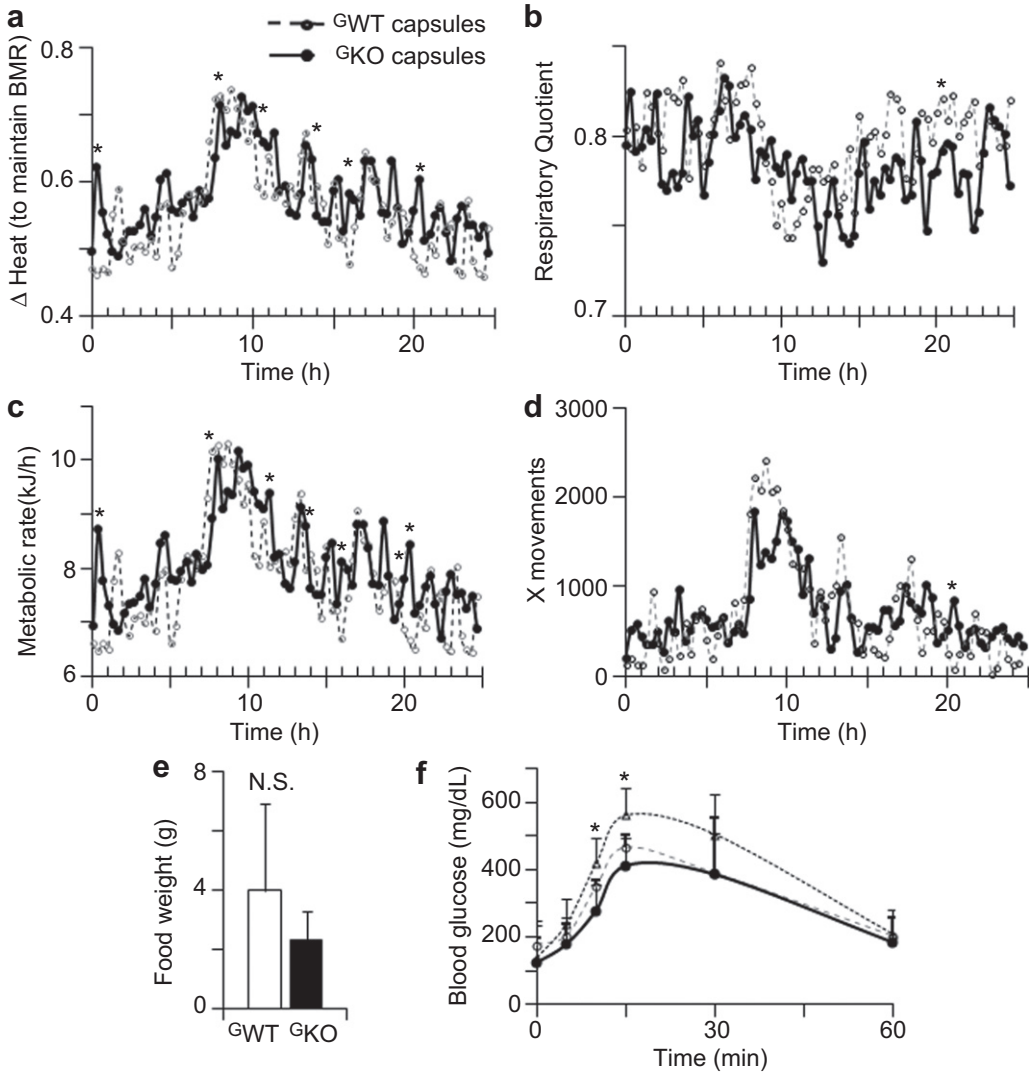

Fig. 7. (a) ΔHeat was quantified in mice (mean, $n = 4$) treated with ^{G}WT (dashed line, open circles) and ^{G}KO (solid line, closed circles) microcapsules for 24 h at the end of the study using metabolic cages (Study 2). ΔHeat values indicate energy liberated by animal to maintain their basal metabolic rate (BMR). *, statistically significant difference between groups measured by Mann–Whitney *U* test. (b–d) Respiratory quotient (b), metabolic rate (c) and X movements (d) were quantified in mice (mean, $n = 4$) treated with ^{G}WT (dashed line, open circles) and ^{G}KO (solid line, closed circles) microcapsules for 24 h at the end of the study using metabolic cages. *, statistically significant difference between groups measured by Mann–Whitney *U* test. (e) Food intake was not significantly different (N.S.) between mice treated with encapsulated ^{G}WT (open bar) and ^{G}KO (black bar) fibroblasts (both, $n = 4$). (f) Glucose tolerance test was performed in mice with mock-injection (triangles, dotted line, $n = 5$) and treated with encapsulated ^{G}WT (open circles, dashed line, $n = 3$) and ^{G}KO (closed circles, solid line, $n = 3$). *, statistically significant difference between control and treated groups measured by Mann–Whitney *U* test.

Identification of gene modifications in the encapsulated cells, which effectively influence lipid metabolism in the host fat tissues, is a prime challenge for encapsulated therapies. Previous attempts to reduce HF diet-induced obesity in mice by leptin-producing microcapsules failed due to the multifactorial nature of this metabolic disorder [2]. Remarkably, fat accumulation was reduced after transplantation of subcutaneous fat [13] and fibroblasts engineered with Prdm16 and C/EBPβ, leading to differentiation of these cells into Ucp1-positive thermocytes [9]. These strategies appear to be less efficient in mice receiving obesogenic diets (reviewed in [5]) due to the dovetailed regulatory relationships among food intake, heat production, energy demand, and oxidative stress/apoptosis. For instance, *Ucp1*$^{-/-}$ and WT mice are equally or more susceptible to HF-diet-induced obesity [41]. Adipose tissue-specific *Ucp1* transgenic mice resist obesity by a complex response that includes atrophy of brown adipocytes and induction of thermocytes with the lower Ucp1 levels in the subcutaneous fat [5,26]. Thermocytes are also present in the visceral fat, but the mechanisms of their induction have not been reported [27].

An *Aldh1a1*$^{-/-}$ phenotype exert several properties that make this gene modification a promising candidate for encapsulation tackling HF diet-induced obesity. Primarily, *Aldh1a1* deficiency increases *Ucp1* mRNA and protein expression levels and number of Ucp1-positive cells in the visceral fat of mice consuming an HF diet. Thus, unlike other genetic modification, *Aldh1a1* deficiency is capable of remodeling of visceral fat.

In vitro *Aldh1a1*$^{-/-}$ fibroblasts (^{G}KO) maintained elevated levels of Ucp1 and other thermogenic genes. Expediently, Ucp1 levels did not reach those seen in brown adipose tissue. Implanted encapsulated ^{G}KO fibroblasts also expressed Ucp1 unlike ^{G}WT fibroblasts. After ^{G}KO implantation, the Ucp1 levels in visceral fat were inversely correlated with both GFP expression and lipid decrease, suggesting participation of ^{G}KO cells in energy dissipation. Encapsulated ^{G}KO cells appeared to act in treated visceral depots, leaving subcutaneous depots unaffected. The depot-specific effect of treatment with this and other types of encapsulated cells needs further investigation as a potential new strategy for the reduction of deleterious fat depots.

An unexpected finding in our study is the distal effects of ^{G}KO microcapsules on the host WT visceral tissue that become populated with numerous Ucp-1 positive cells. *Aldh1a1* deficiency reduces autocrine production of retinoic acid increasing levels of retinaldehyde [28,30] that influence numerous transcription pathways [30,42]. Hypothetically, these pathways can be involved in the production of an unknown cytokine/paracrine hormone responsible for this effect. The investigation of the mechanism responsible for this effect was beyond the scope of this pilot investigation. Another effect requiring further investigation was the marked 10 % weight loss, which was observed only during the first 23d after transplantation of both ^{G}KO and ^{G}WT encapsulated fibroblasts, whereas similar transplantation of empty microcapsules or encapsulated human epithelial kidney cells (HEK293) did not change weights in the host WT mice (data not shown). The absence of weight lowering effects with HEK293 cells argues against non-specific or immune causes for the initial weight loss. It is plausible that the capsules were partially degraded after 23d, which reduced their impact on the weight loss. The inverse correlation between the lipid content in fat depots and GFP protein levels showed that the number of transplanted cells defined lipid and weight loss. It is possible that multiple injections of encapsulated ^{G}KO fibroblasts would increase the magnitude of the visceral fat reduction and prolong the therapeutic action. The substantial weight loss induced by the ^{G}WT fibroblasts could be attributed to subcutaneous phenotype of embryonic fibroblasts [13,35], that seem to induce similar effects in transplantation studies [13].

5. Conclusions

In summary: AP_L can support prolonged survival of fibroblasts with forced lipid catabolism in visceral fat. MRI detects AP_L-encapsulated fibroblasts in vivo, whereas LPMC dissection of encapsulated cells from host tissue enables ex-vivo studies of their interaction. Biological effects of encapsulated ^{G}KO cells conceptually proves the possibility of the preferential visceral fat reduction in spite of HF diet uptake. The microencapsulated ^{G}KO treatment showed several potential advantages compared to current anti-obesity therapies: 1) 23% lipid decrease compared to 15% weight reduction by the most effective pharmaceutical with reported side effects [38]; 2) depot-specific effects, unachievable by other treatments; 3) little to no influx of inflammatory cells and fibrosis; 4) minimally invasive implantation; 5) magnetic resonance imaging (MRI) monitoring in vivo, which enables termination of encapsulated cells treatment by laparoscopy; 6) lipid reduction occurred without changes in lifestyle (HF diet and physical activity). The further development of AP_L encapsulation technology and advancement in cell engineering could provide novel solutions for the treatment of visceral obesity in patients in the future.

Acknowledgments

We would like to express gratitude for excellent service at Laser Capture Molecular Core in OSU medical center directed by Roy, specifically for the laser capturing of encapsulated cells by Bhakthi Deshpande, and Real-Time PCR analysis of these samples by Jennifer Mele. We would also like to thank Dr. Alder, a Director of Nucleic Acid facilities at OSU Wexner Medical Center for diligent mRNA analysis, Dr. Naresh Bal (OSU) for organizing the measurements in metabolic cages, and Dr. Alan Flechtner for the excellent immunohistochemistry services at the Histology/Immunohistochemistry facility in OSU's College of Veterinary Medicine.

This research was supported by the College of Education and Human Ecology (EHE) SEED grant, Food Innovation SEED Grant, and Pilot Industry partnership grant at the center for Clinical and Translational Science, which was supported by Award UL1RR025755 from the National Center Research Resources (Z.O.). The research was supported by EHE Dissertation fellowship (Y.R.). The project described was supported by Award Number UL1RR025755 013000 (Z.O.) from the National Center for Research Resources, RO1 HL 080551 (P.M.) from the National Institute of Health (NIH), Award Number 10POST4150090 (A.M.) from the American Heart Association Great Rivers Affiliate, NS42617, GM77185 and GM69589 (C.S.) from NIH, DK076566 (S.R.) from NIH. Z. X. and L.J.L. thank NSF (EEC-0425626 and EEC-0914790) for financial support. The content is solely the responsibility of the authors and does not necessarily represent the official views of the National Center for Research Resources or the National Institutes of Health.

References

[1] Shao S, Gao Y, Xie B, Xie F, Lim SK, Li G. Correction of hyperglycemia in type 1 diabetic models by transplantation of encapsulated insulin-producing cells derived from mouse embryo progenitor. J Endocrinol 2001;208:245–55.
[2] Oosman SN, Lam AW, Harb G, Unniappan S, Lam NT, Webber T, et al. Treatment of obesity and diabetes in mice by transplant of gut cells engineered to produce leptin. Mol Ther 2008;16:1138–45.
[3] Stratos I, Madry H, Rotter R, Weimer A, Graff J, Cucchiarini M, et al. Fibroblast growth Factor-2-Overexpressing Myoblasts encapsulated in alginate Spheres increase proliferation, reduce Apoptosis, induce adipogenesis, and Enhance Regeneration following skeletal muscle Injury in rats. Tissue Eng 2011;17:2867–77.
[4] Chang TM. Pharmaceutical and therapeutic applications of artificial cells including microencapsulation. Eur J Pharm Biopharm 1998;45:3–8.

[5] Kozak LP. Brown fat and the myth of diet-induced thermogenesis. Cell Metab 2010;11:263–7.
[6] Gupta RK, Rosen ED, Spiegelman BM. Identifying novel transcriptional components controlling energy metabolism. Cell Metab 2011;14:739–45.
[7] Tseng YH, Cypess AM, Kahn CR. Cellular bioenergetics as a target for obesity therapy. Nat Rev Drug Discov 2010;9:465–82.
[8] Cannon B, Nedergaard J. Thermogenesis challenges the adipostat hypothesis for body-weight control. Proc Nutr Soc 2009;68:401–7.
[9] Kajimura S, Seale P, Kubota K, Lunsford E, Frangioni JV, Gygi SP, et al. Initiation of myoblast to brown fat switch by a PRDM16-C/EBP-beta transcriptional complex. Nature 2009;460:1154–8.
[10] Polak P, Cybulski N, Feige JN, Auwerx J, Ruegg MA, Hall MN. Adipose-specific knockout of raptor results in lean mice with enhanced mitochondrial respiration. Cell Metab 2008;8:399–410.
[11] Cannon B, Nedergaard J. Metabolic consequences of the presence or absence of the thermogenic capacity of brown adipose tissue in mice (and probably in humans). Int J Obes (Lond) 2010;34(Suppl. 1):S7–16.
[12] Cypess AM, Kahn CR. Brown fat as a therapy for obesity and diabetes. Curr Opin Endocrinol Diabetes Obes 2010;17:143–9.
[13] Tran TT, Yamamoto Y, Gesta S, Kahn CR. Beneficial effects of subcutaneous fat transplantation on metabolism. Cell Metab 2008;7:410–20.
[14] Tchkonia T, Morbeck DE, Von Zglinicki T, Van Deursen J, Lustgarten J, Scrable H, et al. Fat tissue, aging, and cellular senescence. Aging Cell 2010;9:667–84.
[15] Zhang C, Rexrode KM, van Dam RM, Li TY, Hu FB. Abdominal obesity and the risk of all-cause, cardiovascular, and cancer mortality: sixteen years of follow-up in US women. Circulation 2008;117:1658–67.
[16] Hernandez-Ono A, Monter-Carreola G, Zamora-Gonzalez J, Cardoso-Saldana G, Posadas-Sanchez R, Torres-Tamayo M, et al. Association of visceral fat with coronary risk factors in a population-based sample of postmenopausal women. Int J Obes Relat Metab Disord 2002;26:33–9.
[17] Hotamisligil GS, Johnson RS, Distel RJ, Ellis R, Papaioannou VE, Spiegelman BM. Uncoupling of obesity from insulin resistance through a targeted mutation in aP2, the adipocyte fatty acid binding protein. Science 1996;274:1377–9.
[18] Chu NF, Spiegelman D, Hotamisligil GS, Rifai N, Stampfer M, Rimm EB. Plasma insulin, leptin, and soluble TNF receptors levels in relation to obesity-related atherogenic and thrombogenic cardiovascular disease risk factors among men. Atherosclerosis 2001;157:495–503.
[19] Nanes MS. Tumor necrosis factor-alpha: molecular and cellular mechanisms in skeletal pathology. Gene 2003;321:1–15.
[20] Wucher H, Ciangura C, Poitou C, Czernichow S. Effects of weight loss on bone status after bariatric surgery: association between adipokines and bone markers. Obes Surg 2008;18:58–65.
[21] Hough MR, Reis MD, Singaraja R, Bryce DM, Kamel-Reid S, Dardick I, et al. A model for spontaneous B-lineage lymphomas in IgHmu-HOX11 transgenic mice. Proc Natl Acad Sci U S A 1998;95:13853–8.
[22] Rinomhota AS, Bulugahapitiya DU, French SJ, Caddy CM, Griffiths RW, Ross RJ. Women gain weight and fat mass despite lipectomy at abdominoplasty and breast reduction. Eur J Endocrinol 2008;158:349–52.
[23] Wang YC, McPherson K, Marsh T, Gortmaker SL, Brown M. Health and economic burden of the projected obesity trends in the USA and the UK. Lancet 2011;378:815–25.
[24] Halaas JL, Boozer C, Blair-West J, Fidahusein N, Denton DA, Friedman JM. Physiological response to long-term peripheral and central leptin infusion in lean and obese mice. Proc Natl Acad Sci U S A 1997;94:8878–83.
[25] Heymsfield SB, Greenberg AS, Fujioka K, Dixon RM, Kushner R, Hunt T, et al. Recombinant leptin for weight loss in obese and lean adults: a randomized, controlled, dose-escalation trial. JAMA 1999;282:1568–75.
[26] Stefl B, Janovska A, Hodny Z, Rossmeisl M, Horakova M, Syrovy I, et al. Brown fat is essential for cold-induced thermogenesis but not for obesity resistance in aP2-Ucp mice. Am J Physiol 1998;274:E527–33.
[27] Bostrom P, Wu J, Jedrychowski MP, Korde A, Ye L, Lo JC, et al. A PGC1-alpha-dependent myokine that drives brown-fat-like development of white fat and thermogenesis. Nature 2012;481:463–8.
[28] Ziouzenkova O, Orasanu G, Sharlach M, Akiyama TE, Berger JP, Viereck J, et al. Retinaldehyde represses adipogenesis and diet-induced obesity. Nat Med 2007;13:695–702.
[29] Fan X, Molotkov A, Manabe S, Donmoyer CM, Deltour L, Foglio MH, et al. Targeted disruption of Aldh1a1 (Raldh1) provides evidence for a complex mechanism of retinoic acid synthesis in the developing retina. Mol Cell Biol 2003;23:4637–48.
[30] Reichert B, Yasmeen R, Jeyakumar SM, Yang F, Thomou T, Alder H, et al. Concerted action of aldehyde dehydrogenases influences depot-specific fat formation. Mol Endocrinol 2011;25:799–809.
[31] Schubert KA, Vaanholt LM, Stavasius F, Demas GE, Daan S, Visser GH. Female mice respond differently to costly foraging versus food restriction. J Exp Biol 2008;211:2214–23.
[32] Kuhn DE, Roy S, Radtke J, Khanna S, Sen CK. Laser microdissection and capture of pure cardiomyocytes and fibroblasts from infarcted heart regions: perceived hyperoxia induces p21 in peri-infarct myocytes. Am J Physiol Heart Circ Physiol 2007;292:H1245–53.
[33] Kuhn DE, Roy S, Radtke J, Gupta S, Sen CK. Laser microdissection and pressure-catapulting technique to study gene expression in the reoxygenated myocardium. Am J Physiol Heart Circ Physiol 2006;290:H2625–32.
[34] Zhang X, He H, Yen C, Ho W, Lee LJ. A biodegradable, immunoprotective, dual nanoporous capsule for cell-based therapies. Biomaterials 2008;29:4253–9.
[35] Green H, Meuth M. An established pre-adipose cell line and its differentiation in culture. Cell 1974;3:127–33.
[36] Roy S, Patel D, Khanna S, Gordillo GM, Biswas S, Friedman A, et al. Transcriptome-wide analysis of blood vessels laser captured from human skin and chronic wound-edge tissue. Proc Natl Acad Sci U S A 2007;104:14472–7.
[37] Kang X, Xie Y, Powell HM, James Lee L, Belury MA, Lannutti JJ, et al. Adipogenesis of murine embryonic stem cells in a three-dimensional culture system using electrospun polymer scaffolds. Biomaterials 2007;28:450–8.
[38] Gadde KM, Allison DB, Ryan DH, Peterson CA, Troupin B, Schwiers ML, et al. Effects of low-dose, controlled-release, phentermine plus topiramate combination on weight and associated comorbidities in overweight and obese adults (CONQUER): a randomised, placebo-controlled, phase 3 trial. Lancet 2011;377:1341–52.
[39] Moralejo D, Yanay O, Kernan K, Bailey A, Lernmark A, Osborne W. Sustained glucagon-like peptide 1 expression from encapsulated transduced cells to treat obese diabetic rats. J Biosci Bioeng 2011;111:383–7.
[40] Orive G, Tam SK, Pedraz JL, Halle JP. Biocompatibility of alginate-poly-L-lysine microcapsules for cell therapy. Biomaterials 2006;27:3691–700.
[41] Anunciado-Koza R, Ukropec J, Koza RA, Kozak LP. Inactivation of UCP1 and the glycerol phosphate cycle synergistically increases energy expenditure to resist diet-induced obesity. J Biol Chem 2008;283:27688–97.
[42] Yasmeen R, Jeyakumar SM, Reichert B, Yang F, Ziouzenkova O. The contribution of vitamin A to autocrine regulation of fat depots. Biochim Biophys Acta 2011;1821:190–7.